Atmos. Chem. Phys., 15, 13957–13971, 2015
www.atmos-chem-phys.net/15/13957/2015/
doi:10.5194/acp-15-13957-2015

Atmospheric Chemistry and Physics Open Access EGU

Seasonal variation of ozone and black carbon observed at Paknajol, an urban site in the Kathmandu Valley, Nepal

D. Putero[1], P. Cristofanelli[1], A. Marinoni[1], B. Adhikary[2], R. Duchi[1], S. D. Shrestha[3], G. P. Verza[4], T. C. Landi[1], F. Calzolari[1], M. Busetto[1], G. Agrillo[1], F. Biancofiore[5], P. Di Carlo[5], A. K. Panday[2], M. Rupakheti[6], and P. Bonasoni[1]

[1]CNR-ISAC, National Research Council of Italy – Institute of Atmospheric Sciences and Climate, Via Gobetti 101, 40129 Bologna, Italy
[2]ICIMOD, International Centre for Integrated Mountain Development, G.P.O. Box 3226, Khumaltar, Lalitpur, Kathmandu, Nepal
[3]Ev-K2-CNR Committee, G.P.O. Box 5109, Paknajol, Kathmandu, Nepal
[4]Ev-K2-CNR Committee, Via S. Bernardino 145, 24126 Bergamo, Italy
[5]Center of Excellence CETEMPS, University of L'Aquila, Via Vetoio 1, 67010 Coppito (AQ), Italy
[6]IASS, Institute for Advanced Sustainability Studies, Berliner Strasse 130, 14467 Potsdam, Germany

Correspondence to: D. Putero (d.putero@isac.cnr.it)

Received: 23 June 2015 – Published in Atmos. Chem. Phys. Discuss.: 21 August 2015
Revised: 23 October 2015 – Accepted: 4 December 2015 – Published: 17 December 2015

Abstract. The Kathmandu Valley in south Asia is considered as one of the global "hot spots" in terms of urban air pollution. It is facing severe air quality problems as a result of rapid urbanization and land use change, socioeconomic transformation, and high population growth. In this paper, we present the first full year (February 2013–January 2014) analysis of simultaneous measurements of two short-lived climate forcers/pollutants (SLCF/P), i.e., ozone (O_3) and equivalent black carbon (hereinafter noted as BC) and aerosol number concentration at Paknajol, in the city center of Kathmandu. The diurnal behavior of equivalent BC and aerosol number concentration indicated that local pollution sources represent the major contributions to air pollution in this city. In addition to photochemistry, the planetary boundary layer (PBL) and wind play important roles in determining O_3 variability, as suggested by the analysis of seasonal changes of the diurnal cycles and the correlation with meteorological parameters and aerosol properties. Especially during pre-monsoon, high values of O_3 were found during the afternoon/evening. This could be related to mixing and entrainment processes between upper residual layers and the PBL. The high O_3 concentrations, in particular during pre-monsoon, appeared well related to the impact of major open vegetation fires occurring at the regional scale. On a synoptic-scale perspective, westerly and regional atmospheric circulations appeared to be especially conducive for the occurrence of the high BC and O_3 values. The very high values of SLCF/P, detected during the whole measurement period, indicated persisting adverse air quality conditions, dangerous for the health of over 3 million residents of the Kathmandu Valley, and the environment. Consequently, all of this information may be useful for implementing control measures to mitigate the occurrence of acute pollution levels in the Kathmandu Valley and surrounding area.

1 Introduction

Air pollution is a major environmental challenge in several regions of the world, defined as "hot spots" (Monks et al., 2009). In south Asia, by using in situ measurements, chemical transport models, and satellite observations, Ramanathan et al. (2007) identified layers of regional-scale plumes of atmospheric pollutants that extended from the Himalayas to the northern Indian Ocean, including high levels of short-lived climate forcers/pollutants (SLCF/P), such as black carbon (BC) and ozone (UNEP and WMO, 2011). Several significant implications of these compounds were recognized for the global climate (Ramanathan and Carmichael, 2008),

regional climate and crop yields, and for human health (Shindell et al., 2012).

The Kathmandu Valley in Nepal, the largest metropolitan region at the Himalayan foothills (one of the most polluted but still least sampled regions of the world), represents one of the regional hot spots in terms of air pollution. This area, having a cross section of about 20 km north to south and 30 km east to west, comprises three administrative districts, Kathmandu, Lalitpur, and Bhaktapur, and has undergone rapid but unplanned urbanization due to high population growth, dramatic land use changes, and socioeconomic transformation, thus facing severe air pollution problems. Over the past quarter of a century, the Kathmandu Valley's population has quadrupled to more than 3 million. Between 1990 and 2014 the total vehicle fleet grew from 45 871 to more than 700 000, with the number of motorcycles having the highest annual growth rate of 16 % during the period (Faiz et al., 2006; Shrestha et al., 2013). Furthermore, by using an energy system model, Shrestha and Rajbhandari (2010) indicated that the total energy consumption in the Kathmandu Valley is expected to increase at an average growth rate of 3.2 % in the period from 2005 to 2050. By 2050, there will be an increase in the energy consumption of 30, 25, and 22 % for the shares of transport, industrial, and commercial sectors, respectively. In the city center of Kathmandu the air quality is so bad that Nepal's own national ambient air quality standards are only met on about 40 days per year; during the rest of the year, the particulate matter exceeds the limit considered harmful. The sizable emission of air pollutants in the Kathmandu Valley is of concern for local and regional air quality and climate; however, it is still a manageable size in terms of potential interventions to address serious air pollution problems in the valley. The relative importance of local and regional emission sources has not been well quantified yet, making it difficult to design mitigation strategies that will have a large impact and still be cost-effective. Therefore, an improved scientific understanding of the main sources and impacts of air pollution in the region is a prerequisite for designing effective mitigation options.

In the recent past, several studies have presented measurements of various atmospheric compounds in the Kathmandu Valley (e.g., Sharma et al., 2012; Panday and Prinn, 2009; Panday et al., 2009; Pudasainee et al., 2006; Giri et al., 2006; Sharma, 1997; Shrestha and Malla, 1996), all suggesting that air pollution in Kathmandu has harmful effects on human health (leading to bronchitis, and throat and chest diseases), crop productivity, and also tourism income in Nepal, Kathmandu being the heart of Nepalese culture, art, and architecture. However, none of them presented simultaneous observations of key SLCF/P across seasons.

In order to provide continuous measurements of atmospheric composition variability, a measurement site was installed in 2013 at Paknajol, in the tourist area of the city of Kathmandu. This has enabled us to achieve a more comprehensive understanding of the dynamics of air pollution and related emissions in the Kathmandu Valley, and to constitute a scientific basis in order to support the local implementation of mitigation actions. These measurements were carried out as part of the SusKat-ABC (A Sustainable Atmosphere for the Kathmandu Valley – Atmospheric Brown Cloud) campaign in Nepal, the second largest international air pollution measurement campaign ever carried out in southern Asia, whose aim is to provide the most detailed air pollution measurements to date for the Kathmandu Valley and the surrounding region (Rupakheti et al., 2015).

2 Materials and methods

2.1 Measurement site and instrumental setup

Kathmandu is located in a broad basin at the foothills of the central Himalayas, the valley floor at an average altitude of 1300 m a.s.l. The mountains surrounding the valley have peaks ranging from 2000 to 2800 m a.s.l. Neighboring valleys to the west, north, northeast, and south have substantially lower elevations. The meteorology of the Kathmandu Valley is influenced by large-scale features, western disturbances, and the south Asian summer monsoon, as well as local mountain–valley circulations. As reported by Panday and Prinn (2009) and Panday et al. (2009), during the dry season the diurnal cycle of air pollutants (CO, O_3, PM_{10}) is strongly affected by local meteorology connected to the evolution of the convective planetary boundary layer (PBL) and thermal wind flows along the flanks of the mountains surrounding the valley.

The Paknajol site is located (27°43′4″ N, 85°18′32″ E; 1380 m a.s.l.) near the edge of Kathmandu's tourist district of Thamel. The sampling site is on the terrace (about 25 m a.g.l.) of the Ev-K2-CNR representative office. This is the highest building in the block; thus it has a 360° free horizon of at least 300 m. The instruments are located in an air-conditioned room, in order to maintain the correct operating conditions. A UPS – which signifies an uninterruptible power supply – guarantees the continuous measurements in case of (frequent) blackout events; there may be power cuts of up to 18 h a day, especially during the winter months. The sampling heads are placed on the roof just outside this room. The measurement activities, including aerosol and trace gas measurements, were started in February 2013.

The following instruments are used for continuous measurements.

1. A UV-absorption analyzer (TEI 49i, Thermo Environmental) is used to collect surface O_3 measurements. These are linked to the World Meteorological Organization (WMO)/Global Atmosphere Watch (GAW) reference scale (Standard Reference Photometer; SRP 15; see Klausen et al., 2003) hosted at the GAW World Calibration Centre (WCC) at EMPA (Switzerland), via direct comparison with the CNR-ISAC laboratory

standard hosted at the Mt. Cimone WMO/GAW global station (Italy). The experimental setup is similar to that described in Cristofanelli et al. (2010).

2. Aerosol light absorption and BC, derived by using the mass absorption efficiency of $6.5\,m^2\,g^{-1}$, are measured through a Multi-Angle Absorption Photometer (MAAP 5012, Thermo Electron Corporation). For more details, see Marinoni et al. (2010). The correction described in Hyvärinen et al. (2013) for the measurement artifact, affecting the instrument's accuracy at high BC concentrations, was applied. A PM_{10} cutoff size was used in the sampling head.

3. Meteorological parameters (atmospheric pressure and temperature, wind speed and direction, relative humidity (RH), and precipitation) are monitored using an automatic weather station (WXT 425, Vaisala). Global solar radiation is monitored using a pyranometer (CMP21, Kipp&Zonen).

4. Aerosol number concentration and size distribution (in the range $0.28\,\mu m \leq D_p < 10\,\mu m$, D_p being the geometric diameter of particles) are measured using an optical particle counter (OPC Monitor, FAI Instruments), which uses a laser light scattering technique ($\lambda = 780\,nm$). The OPC optical diameters (divided into eight bins) are then converted into geometric diameters, assuming that particles are spherical. In order to minimize biases related to coincidence errors, but also to reduce RH and dry aerosol particles, the air sample is subjected to a dilution process, whose dilution factor can be varied by modifying the dilution flow rate (from 0 to $4\,L\,min^{-1}$).

5. Online PM_{10} and PM_1 are measured (with a 24 h resolution), using the β-absorption technique, with a medium-volume ($2.3\,m^3\,h^{-1}$) sampler (SWAM Dual Channel, FAI Instruments). The instrument is equipped with two 12 V back-up batteries, in order to complete measurements in case of electricity power breaks. From 1 April 2013 a PM_1 sampling head has been installed, replacing the $PM_{2.5}$ one.

All measurements presented in this work refer to Nepal standard time (NST, UTC + 05:45); data are stored and fully validated on a 1 min basis, then averaged to a common time base of 60 min, and expressed in standard temperature and pressure = (0 °C and 1013 hPa) conditions. With the purpose of aggregating data to hourly average values, 50 % data coverage criteria were used; i.e., at least 50 % coverage of the data sampling period was required to give a 1 h average.

2.2 Back trajectories calculation

In order to describe the synoptic-scale atmospheric circulation scenarios over the Kathmandu Valley and the surrounding region, isentropic 5-day back trajectories have been used, computed by the HYSPLIT model (Draxler and Hess, 1998) every 6 h (at 05:45, 11:45, 17:45, and 23:45 NST). With the aim of minimizing the effect of the complex topography and to provide a description of the large-scale circulation in the free troposphere, calculations were initialized at 600 hPa. The model calculations are based on the Global Data Assimilation System (GDAS) meteorological field produced by NCEP Reanalysis data, with a horizontal resolution of $1^\circ \times 1^\circ$. In order to aggregate the back trajectories of common origin, and better characterize the synoptic-scale circulation occurring at Paknajol, a cluster aggregation technique (Draxler, 1999) has been applied to the back trajectories. Basically, at each step of the process, the appropriate number of clusters was identified, based on the variations of several statistical parameters; by maximizing between-group variance and minimizing within-group variance, this methodology might identify similar air-mass back trajectories and aggregate them.

2.3 Recurrent model analysis

To understand how photochemistry and dynamics affect the variation of O_3 mixing ratios and to comprehend the origin of elevated O_3 levels in the afternoon and evening hours during the pre-monsoon period, we used a recurrent neural network model. These models allow us to simulate the nonlinear relationship between O_3 and meteorological parameters that are proxies of photochemistry and dynamics (Lönnblad et al., 1992; Elman, 1990). Considering the strong role of meteorological conditions and photochemistry on the variations of O_3 mixing ratios (Pudasainee et al., 2006; Di Carlo et al., 2007) and the fact that meteorological effects usually last for more than 1 day, the more complex architecture of the neural network that uses the recurrent approach takes into account the multi-day effect of meteorology, as well as diurnal boundary layer cycles (Biancofiore et al., 2015). The model uses the observed pressure, temperature, RH, solar radiation, wind velocity and direction, and BC concentrations as input to simulate the O_3 mixing ratio (Biancofiore et al., 2015). The inclusion of a sub-group of these proxies allows us to distinguish between the role of dynamics and that of photochemistry in the observed variations of O_3 mixing ratio.

3 Results

3.1 Meteorological characterization

The Paknajol area is strongly influenced by local traffic and urban emissions, as it is located near the edge of Kathmandu's tourist center, and near a major thoroughfare. Meteorological observations at the sampling site help in better describing the seasonal and diurnal variability of the air pollutants and SLCF/P in the Kathmandu Valley.

With the aim of identifying the regional transition of the monsoon seasonal regimes, we considered meteorological

Table 1. Onset and decay dates of the different seasons selected in this work.

Season	Start day–end day
Pre-monsoon	1 February–12 May 2013
Monsoon	13 May–6 October 2013
Post-monsoon	7 October–26 October 2013
Winter	27 October 2013–31 January 2014

observations carried out at the Nepal Climate Observatory-Pyramid (NCO-P) station, located at 5079 m a.s.l. near Mt. Everest in the Himalayas. As shown by Bonasoni et al. (2010), the variability of meteorological parameters (i.e., RH and meridional wind component) observed at NCO-P can be used to derive the onset and withdrawal dates of the different seasons on the south side of the Himalayan range (where NCO-P is located). Moreover, as described in the annual report of the India Meteorological Department (IMD, 2014), the seasonal advance of the south Asian monsoon cycle did not differ too much between the location of NCO-P and Kathmandu. Table 1 reports the start and withdrawal dates of each season (pre-monsoon, monsoon, post-monsoon, winter) for the period considered in this study.

Figure 1 shows the variability of the meteorological parameters measured at Paknajol from February 2013 to the end of January 2014. Hourly atmospheric temperature (T, Fig. 1a) values never exceeded 29.5 °C, while minima never dropped below 3.5 °C. Over the whole measurement period, T had an average value of 18.7 ± 5.6 °C (hereinafter, average values are indicated as average $\pm$ 1 standard deviation). T was characterized by an evident diurnal cycle, with values peaking in the middle of the day and a minimum in the early morning. Atmospheric pressure (P, Fig. 1b, average value: 865.3 ± 4.1 hPa) showed its minimum values during the summer season, which is characterized by the presence of the monsoon trough over Nepal, accompanied by frequent and intense showers, reaching up to 47 mm h^{-1} (Fig. 1d). P is characterized by a semi-diurnal cycle, with two minima (at 04:00 and 16:00) and two maxima (at 10:00 and 22:00), with average amplitudes ranging from 1.2 hPa (pre-monsoon) to 3.5 hPa (post-monsoon). RH values (Fig. 1c, average value: 67.1 ± 17.0 %) were high during all of the measurement period, rarely decreasing below 20 % (50 % during the summer monsoon season); it has to be noted that during winter, RH values swing from very high to very low, thus presenting the widest diurnal cycle among all of the seasons. Saturation conditions (RH equal to 95 % or higher) were mainly reached during the most intense rainfalls. In agreement with rainfall reported in Panday and Prinn (2009), about 90 % of annual rainfall was observed during June–August. Figure 1e and f show wind speed and direction, respectively. The sampling site was characterized by low wind speeds, with the majority of winds from the W–NW sector and a

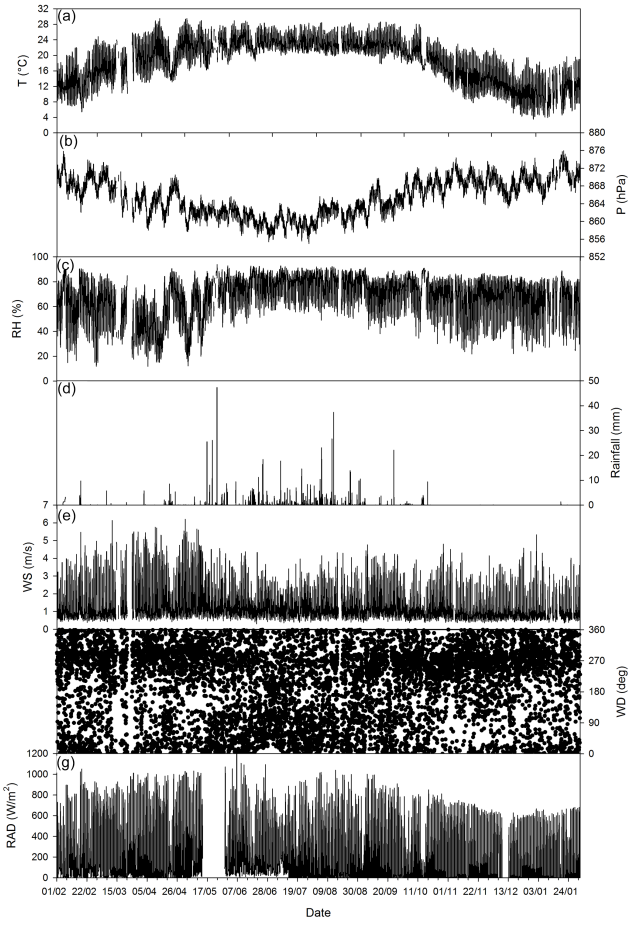

Figure 1. Time series of hourly atmospheric temperature (T, panel **a**), pressure (P, panel **b**), relative humidity (RH, panel **c**), precipitation **(d)**, wind speed (WS, panel **e**), wind direction (WD, panel **f**) and solar radiation (RAD, panel **g**) measured at Paknajol.

secondary contribution from the W–SW sector (see Fig. S1, Supplement). As shown in Panday and Prinn (2009) and Panday et al. (2009), nights were characterized by low wind speeds (maximum speed: 4 m s^{-1}) coming from several directions, mainly explained by katabatic winds descending from the mountain slopes at the edge of the Kathmandu Valley rim; however, during the afternoon, stronger winds (reaching up to 6.5 m s^{-1}) occurred at the measurement site, which was swept by westerly/northwesterly winds which entered through the western passes.

3.2 SLCF/P seasonal and diurnal cycle

The hourly average (along with daily averages) time series for O_3, BC, and particle number concentration are shown in Fig. 2. Figure 3 shows the diurnal variability of these pollutants across the seasons, while seasonal average values are presented in Table 2.

Similarly to other polluted cities, the rush hours and PBL dynamics result in the distinct morning and evening peaks:

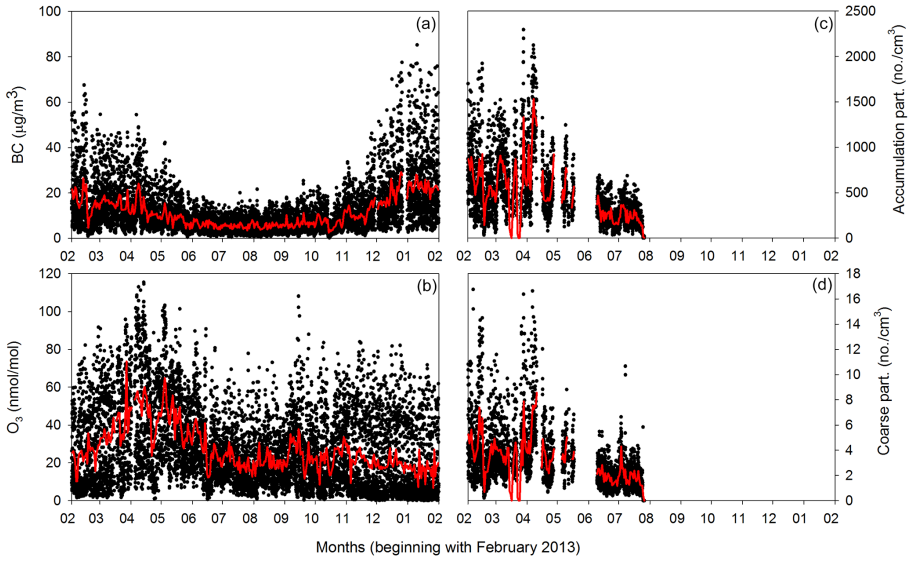

Figure 2. Time series of hourly concentrations of equivalent black carbon **(a)**, surface ozone **(b)**, accumulation **(c)**, and coarse particles **(d)** recorded at Paknajol. Red lines denote daily averages.

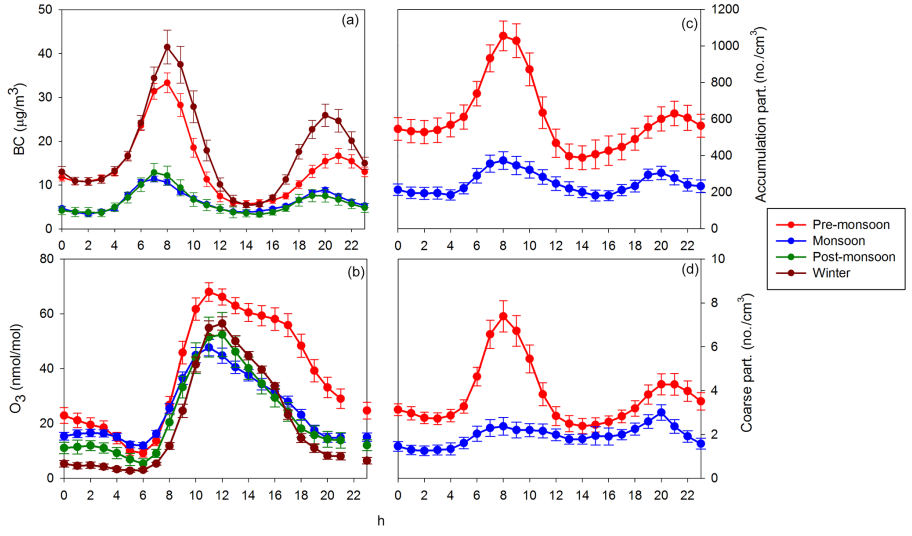

Figure 3. Average seasonal diurnal variation for equivalent black carbon **(a)**, surface ozone **(b)**, accumulation **(c)**, and coarse particles **(d)** recorded at Paknajol. The error bars denote the expanded uncertainties ($p < 0.05$) of the mean.

an increase in traffic activities and congestion, an increase in emissions from cooling/heating activities (LPG, kerosene, and firewood), as well as a decrease in the PBL. The primary emission indicators, i.e., BC and aerosol particle number, reveal such activities. Industries, especially brick kilns, and open garbage burning also contribute to poor air quality in the Kathmandu Valley.

The average value of BC (Fig. 2a) over the whole measurement period was $11.6 \pm 10.7\,\mu g\,m^{-3}$. The highest BC concentrations were observed during pre-monsoon and winter seasons (Table 2), with daily values often exceeding $20\,\mu g\,m^{-3}$; while the lowest values occurred during the monsoon season (the lowest daily value recorded was $2.5\,\mu g\,m^{-3}$). These levels are slightly higher than what is reported in a previous study by Sharma et al. (2012) at Pulchowk Campus, in which they reported an average BC of $8.4 \pm 5.1\,\mu g\,m^{-3}$, over a year-long study period spanning between May 2009 and April 2010. Another study by Shrestha et al. (2010) reported far lower values of elemental carbon concentration ($1.7 \pm 0.6\,\mu g\,m^{-3}$) for an urban site 30 km southeast (downwind) of the Kathmandu Valley, during the 2009 pre-monsoon season. The highest seasonal values, observed during winter/pre-monsoon, can be attributed to several factors: an increase in emissions from domestic heating, the use

Table 2. Average values (± standard deviation) of the pollutants, computed for the different seasons selected by the periods of Table 1.

	O_3 (nmol mol^{-1})	BC (μg m^{-3})	Accum. (no. cm^{-3})	Coarse (no. cm^{-3})	PM_1 (μg m^{-3})	PM_{10} (μg m^{-3})
Pre-monsoon	38.0 ± 25.6	14.5 ± 10.4	668 ± 383	4.2 ± 2.5	98 ± 83	241 ± 134
Monsoon	24.9 ± 16.5	6.3 ± 3.8	250 ± 141	1.9 ± 1.1	32 ± 12	107 ± 37
Post-monsoon	22.8 ± 17.0	6.2 ± 3.9	–	–	26 ± 10	101 ± 38
Winter	20.0 ± 19.8	18.3 ± 14.1	–	–	74 ± 26	320 ± 75
All	27.0 ± 21.3	11.6 ± 10.7	505 ± 372	3.3 ± 2.4	48 ± 42	169 ± 113

of small but numerous gensets during extended hours with power cuts, the operation of over 100 brick kilns in the valley, refuse burning, as well as lower PBL and lower wet deposition of pollutants in winter months compared to the summer months with intense heat and rainfall. The average diurnal variation in BC concentrations in the different seasons is shown in Fig. 3a. The typical diurnal variation for BC, as also shown in Sharma et al. (2012), reflects the BC profile for an urban site, presenting two daily maxima, with a prominent peak in the morning (between 07:00 and 08:00), and a second one in the evening (between 20:00 and 21:00), as well as two minima at night (between 01:00 and 02:00) and in the afternoon (between 14:00 and 15:00). These two daily peaks reveal the start and build-up of emissions due to local anthropogenic activities, such as traffic and cooking activities. Moreover, also a meteorological component cannot be ignored: this is due to the presence of katabatic winds that lead to the uplift of surface polluted air masses during the night. The following build-up of the morning mixed layer favors the downward mixing of pollutants back to the bottom of the valley (Panday and Prinn, 2009; Panday et al., 2009). This diurnal cycle was observed in all four seasons but the peak values were much higher in winter and pre-monsoon seasons (morning peaks: 41.4 and 33.3 μg m^{-3}, respectively) compared to the post-monsoon and monsoon seasons (12.9 and 11.4 μg m^{-3}, respectively).

Surface ozone (O_3) had an average value of 27.0 ± 21.3 nmol mol^{-1} (1 nmol mol^{-1} is equivalent to 1 ppb) over the whole measurement period (Fig. 2b). The highest O_3 was observed during the pre-monsoon season, while the lowest values were reached during the winter season (Table 2). This spring peak is a feature widely present in south Asia and the Himalayas (see e.g., Cristofanelli et al., 2010; Agrawal et al., 2008). Pudasainee et al. (2006), using measurements made at Lalitpur, an adjacent city to the Kathmandu municipality, suggested that variations of solar radiation, ambient temperature, and precursors (such as NO_x and VOCs) can together explain 93 % of the variation in measured ground level O_3 at Kathmandu. Following Chevalier et al. (2007), with the aim of attributing the fraction of O_3, BC, accumulation, and coarse particles' variability related to day-to-day and diurnal-scale processes, we calculated the ratio of daily/hourly standard deviations. The obtained values (0.54 for O_3, 0.59 for BC, 0.81 for accumulation, and 0.71 for coarse particles) indicated that both diurnal and day-to-day variations are important to explain O_3, BC, and particle number variations at Paknajol. O_3 diurnal variation is shown in Fig. 3b: a peak in O_3 mixing ratios characterized the central part of the day (between 11:00 and 13:00), while a minimum was observed in the morning (between 05:00 and 06:00). This diurnal variation is typical for polluted urban sites (Jacobson, 2002) and can be explained in terms of local O_3 photochemistry production and removal processes as well as PBL dynamic and vertical air-mass mixing, as discussed in Sect. 3.4.

Particle number concentrations of accumulation ($0.28\,\mu m \leq D_p < 1\,\mu m$) and coarse ($1\,\mu m \leq D_p < 10\,\mu m$) particles are reported in Fig. 2 (panels c and d, respectively). Unfortunately, due to instrumental failures, no measurements were available after 27 July 2013; only two seasons were covered, i.e., pre-monsoon and monsoon. The average values over the available time period were 505 ± 372 cm^{-3} for the accumulation particles and 3.3 ± 2.4 cm^{-3} for the coarse particles. Accumulation and coarse particle concentrations were high during the pre-monsoon season and far lower during the monsoon (Table 2). The average seasonal diurnal cycles (Fig. 3c for accumulation and Fig. 3d for coarse) were somewhat similar to that of BC, presenting two daily peaks, in correspondence to the start of working activities and traffic rush hours, thus indicating common anthropogenic emission sources and similar meteorological influences. The similar behavior between accumulation and coarse particle number concentrations suggests likely common origins, indicating that the main fraction of coarse particles is linked to the resuspension of road dust or ash from local combustion and not to mineral dust transport from desert areas. During the pre-monsoon, the morning peak was higher (1054 cm^{-3} for accumulation and 7.4 cm^{-3} for coarse) than the one recorded in the evening (629 and 4.3 cm^{-3}, respectively). The same was true for the accumulation mode even during the monsoon season, although the difference between the two peaks showed smaller amplitude. For coarse particles, however, the evening peak appeared to be higher than the morning peak during the wet season. This can be explained by considering the wet conditions which usually characterized Kathmandu during nighttime in this season; moreover, it has to be noted that this phenomenon may be combined with aerosol drying from the dilution system of the OPC that is not sufficient. Most of the rain

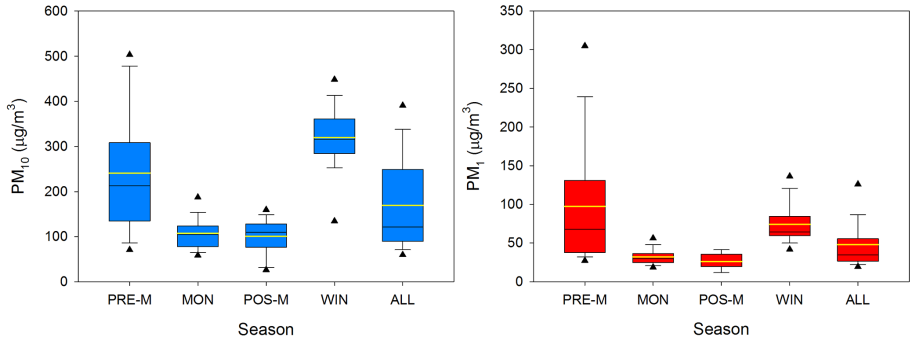

Figure 4. Box-and-whisker plot for PM_{10} (left panel) and PM_1 (right panel) concentrations at Paknajol, segregated by season (PRE-M: pre-monsoon, MON: monsoon, POS-M: post-monsoon, WIN: winter, and ALL: the whole measurement period). The boxes and whiskers denote the 10th, 25th, 75th, and 90th percentiles of PM values; triangles denote the 5th and 95th percentiles. The median (mean) value is denoted by the black (yellow) line.

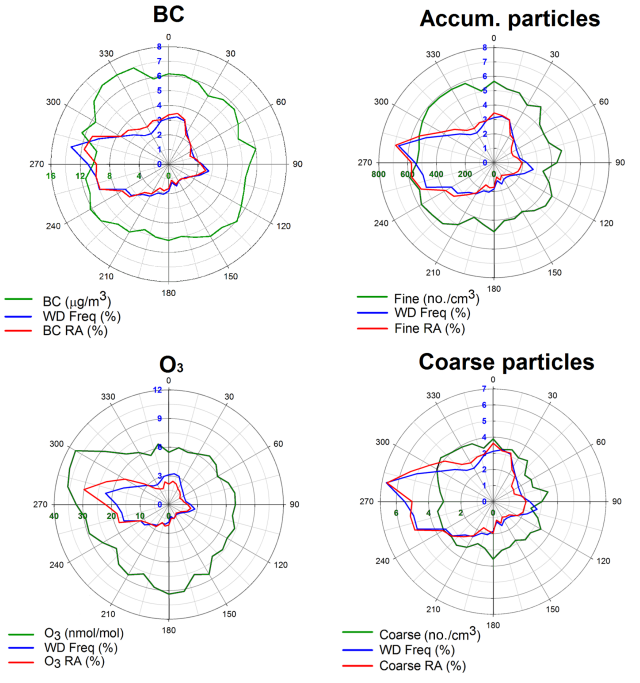

Figure 5. Relation between BC, O_3 (left column), accumulation, and coarse particles (right column), and wind direction for Paknajol. The green line represents the mean of the respective pollutant per 10° WD interval, the blue line is the relative frequency of WD, and the red line is the relative abundance of the chosen pollutant, weighted by the WD frequency, as explained in Gilge et al. (2010).

occurs during the nighttime, and the wet surface in the early morning prevents emission of roadside dust and soil. As the day evolves, moisture is more efficiently evaporated, leaving dry dust and soil to be resuspended by traffic or winds, thus leading to the appearance of a larger evening peak for coarse particle number.

Figure 4 shows the seasonal box-and-whisker plot for PM_{10} and PM_1 recorded at Paknajol. Prior to 1 April 2013, a $PM_{2.5}$ sampling head was installed in place of the PM_1 one. By considering the whole sampling period, PM_{10} had an average value of $169 \pm 113\ \mu g\,m^{-3}$, which is comparable to the value found by Giri et al. (2006), $133.7 \pm 70.3\ \mu g\,m^{-3}$, computed over the period 2003–2005 for the Thamel measurement site (not far from Paknajol), or to the values found in Aryal et al. (2008), which range from 170 to $230\ \mu g\,m^{-3}$ (annual averages) for two busy traffic area stations in Kathmandu. Our value appears slightly higher than those of Giri et al. (2006). This is in line with the increasing urbanization and the growth of the total vehicle fleet which occurred in the Kathmandu Valley. The maximum seasonal average of PM_{10} was found during winter, while minima occurred during monsoon and post-monsoon seasons (Table 2). $PM_{2.5}$ presented an average value of $195 \pm 83\ \mu g\,m^{-3}$ over its short time period (17 days), while PM_1 had an average value of $48 \pm 42\ \mu g\,m^{-3}$, with the maximum values during the pre-monsoon and winter seasons and significantly lower values during monsoon and post-monsoon (Table 2). Over the whole measurement period, the ratio PM_1 / PM_{10} was 0.29 ± 0.10, indicating a large contribution of coarse particles to the total aerosol mass. This aerosol mass concentration ratio, whose values were the highest during the pre-monsoon (0.39 ± 0.09) and lowest during winter (0.21 ± 0.05), is similar to the ratios observed for arid sites (Shahsavani et al., 2012; Lundgren et al., 1996), for sites affected both by dust storms originating in Asia (Claiborn et al., 2000), strong African dust outbreak episodes (Alastuey et al., 2005), and dusty roads (Colbeck et al., 2011). Similar ratios were observed also in other large municipalities in south Asia, such as Bilaspur (0.24, Deshmukh et al., 2010) or Raipur (0.28, Deshmukh et al., 2013) in India, or Nanjing (0.34, Wang et al., 2003) in China. In the European cities this ratio is generally higher than in Asia.

3.3 SLCF/P behavior as a function of wind direction

We highlighted the wind sector which mostly contributed to the occurrence of high SLCF/P values at the measurement

site, as presented in Fig. 5. Here, the angular distribution of the pollutants averaged over WD intervals of 10° (green lines) is shown. Also reported in the figure are the distributions of the frequency of wind directions (blue) and the relative abundance of the pollutants (red), weighted by the wind directions, computed according to Gilge et al. (2010). These analyses refer to the whole investigation period and no significant differences were observed, neither by categorizing data as a function of the different seasons, nor by the time of day. WD behavior has already been presented in Sect. 3.1; BC and aerosol particle number (both accumulation and coarse) average values did not show any dependence as a function of wind direction. This is conceivable considering that Paknajol is located in the middle of several pollution sources. O_3 angular mean values (green line) showed enhanced values from the W–NW sector (35 nmol mol^{-1} on average). This leads to a small distortion of the O_3 contribution away from the distribution of the wind directions (peaking at 270°). 48 % of the total O_3 recorded at Paknajol station was enclosed in the 240–320° wind sector, which perfectly matches the direction from a mountain pass from where, according to Panday and Prinn (2009), air masses can be transported during daytime towards Kathmandu due to thermal transport, indicating the arrival of regional polluted air masses.

3.4 Correlation analysis among SLCF/P

By looking at the diurnal variations presented in Fig. 3, the first peak in BC and aerosol particles can be explained in terms of increased emission (traffic and cooking activity) under atmospheric stable conditions and low PBL height or with an additional contribution of down-mixing as the nighttime stable boundary layer breaks up (Panday and Prinn, 2009). Dilution within the higher PBL, arrival of cleaner air from west of the Kathmandu Valley, and decrease of emissions can explain the daily minimum in aerosol and BC observed from 11:00 to 17:00. Conversely, the peak in O_3 can be explained in terms of enhanced photochemical production (with respect to nighttime or early morning), as well as in terms of downward vertical mixing of polluted regional air masses from the free troposphere or the nighttime residual layer. When the PBL height starts to decline due to the diurnal decrease of solar radiation and soil heating, along with the increased emissions of evening traffic and cooking activities, a secondary peak in BC aerosol is observed from 18:00 to 22:00. Titration with NO, dry deposition, and less efficient vertical mixing within a more stable PBL lead to the decrease of O_3 which finally results in the nighttime minimum, when BC and aerosol particles also present the lowest concentrations due to the decrease of traffic and domestic emissions. Moreover, since measurements were taken on the roof of a tall building, in the presence of a stable nighttime atmosphere, it may be difficult to capture near-surface pollution. These behaviors led to a negative correlation between hourly BC and O_3 (Table 3), which was almost constant over all of the considered seasons. The O_3 decrease after the noon peak was faster during winter and post-monsoon seasons, while it was more gradual during pre-monsoon and monsoon. Moreover, during the pre-monsoon season, a "bump" in O_3 mixing ratios (> 50 nmol mol^{-1}) was observed during the afternoon (between 11:00 and 17:00; Fig. 3). The simultaneous decreases of BC and aerosol particle concentrations support a strong role of downward vertical mixing in enhancing O_3 and decreasing primary pollutants (BC and aerosol particles). The important role of dynamics in influencing SLCF/P variability is confirmed by the negative (positive) correlation between wind speed and BC (O_3). The correlation coefficients (r) are higher by considering daily average values (Table 3), supporting the role of day-to-day meteorology in influencing the SLCF/P.

BC showed significantly higher hourly correlation with accumulation and coarse particles (0.86 and 0.87, respectively), which was lower during the wet season (0.66), strongly supporting common sources and processes that influence their variability (i.e., traffic sources and PBL dynamics). The lower correlation can be explained in terms of different hygroscopicities of BC with respect to other aerosol particles (see Marinoni et al., 2010), which can lead to a lower scavenging efficiency of BC, with respect to other inorganic and organic species, that has been proved especially for non-aged BC (Cozic et al., 2007). Due to the lack of data, no information about the variation of the correlation coefficients computed between accumulation and coarse particles could be given other than during pre-monsoon and monsoon seasons. The high correlation coefficient between BC and accumulation (and coarse) particles could however indicate that BC can be used as an indicator of primary pollution, even when measurements by the OPC are lacking.

O_3 showed high correlation with solar radiation (0.71 for hourly and 0.56 for daily values) and temperature, which is considered as a proxy for seasons (0.51 and 0.32); this is somewhat expected for an urban site like Kathmandu, where photochemistry and PBL dynamics (indirectly driven by solar radiation and temperature behavior) play an important role in determining O_3 variability (Pudasainee et al., 2006). The correlation with solar radiation exhibited some variability during the year, giving the lowest values (0.59 for hourly values and 0.06 for daily values) during the pre-monsoon season, possibly supporting the enhanced role of atmospheric transport and dynamics in influencing O_3 with respect to photochemistry. Apparently, this agrees only in part with the results shown in Pudasainee et al. (2006), in which the authors argued that the "flat peak" in O_3 concentrations during the pre-monsoon is mainly due to abundance of solar radiation and higher temperature (justified by high correlation coefficient values).

In order to distinguish the chemical effects from the boundary layer dynamics, we also computed correlation coefficients limiting the data to convective hours only (i.e., between 11:00 and 17:00, according to the wind speed and

Table 3. Correlation coefficients (r) between several parameters (BC, O_3, accumulation and coarse particles, WS, T, and solar radiation (RAD)) for hourly and daily (in parentheses) values, over the whole sampling period.

	O_3	BC	Acc.	Coarse	WS	T	RAD
O_3	–	−0.21 (−0.04)	0.11 (0.43)	0.07 (0.41)	0.54 (0.65)	0.51 (0.32)	0.71 (0.56)
BC	−0.21 (−0.04)	–	0.86 (0.78)	0.87 (0.74)	−0.35 (−0.21)	−0.56 (−0.58)	−0.10 (−0.15)
Acc.	0.11 (0.43)	0.86 (0.78)	–	0.86 (0.91)	−0.22 (0.12)	−0.39 (−0.38)	−0.02 (−0.06)
Coarse	0.07 (0.41)	0.87 (0.74)	0.86 (0.91)	–	−0.21 (0.18)	−0.31 (−0.35)	−0.07 (−0.03)
WS	0.54 (0.65)	−0.35 (−0.21)	−0.22 (0.12)	−0.21 (0.18)	–	0.45 (0.41)	0.40 (0.56)
T	0.51 (0.32)	−0.56 (−0.78)	−0.39 (−0.38)	−0.31 (−0.35)	0.45 (0.41)	–	0.43 (0.31)
RAD	0.71 (0.56)	−0.10 (−0.15)	−0.02 (−0.06)	−0.01 (−0.03)	0.40 (0.56)	0.43 (0.31)	–

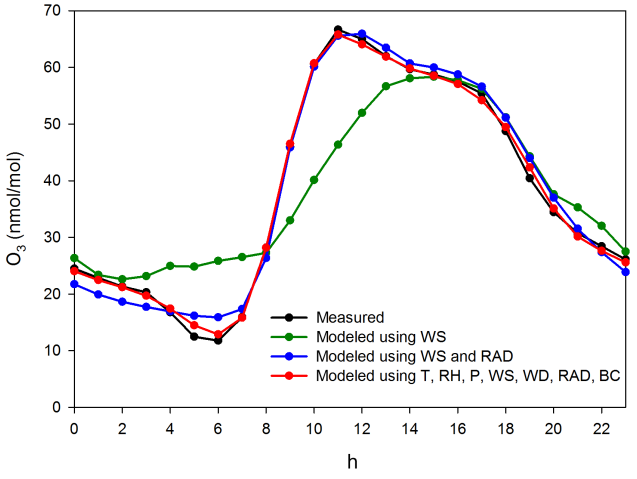

Figure 6. Average seasonal diurnal variation of O_3 concentrations for the pre-monsoon period, compared with modeled O_3 using different input parameters (T, RH, P, WS, WD, RAD, and BC).

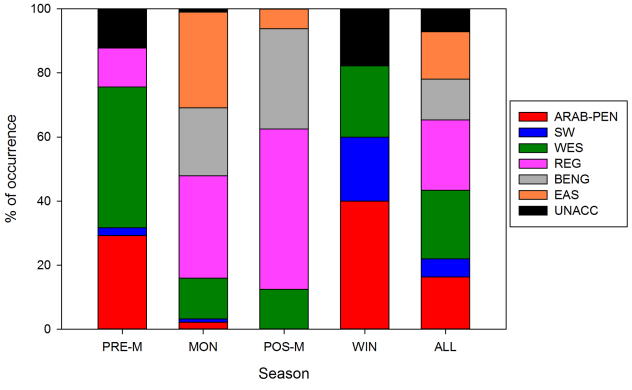

Figure 7. Percentage of occurrence registered by the six different back-trajectory clusters considered in this work, divided by season (PRE-M: pre-monsoon, MON: monsoon, POS-M: post-monsoon, WIN: winter, and ALL: considering the whole measurement period). Abbreviations for clusters are as follows: ARAB-PEN – Arabian Peninsula, SW – southwesterly, WES – western, REG – regional, BENG – Bay of Bengal, EAS – eastern, and UNACC – unaccounted for.

solar radiation diurnal variations). The slightly weaker correlation between BC and accumulation particle number and, conversely, the increase in correlation between O_3 and accumulation particle number, may indicate the role of other processes (e.g., secondary aerosol production) occurring in the air masses which characterize this specific time span (Table S1, Supplement). In particular, we suppose that aged air masses rich in secondary pollutants (i.e., O_3 and aerosol) can be transported to the measurement site in the afternoon mixed layer.

Here, we argue that mixing processes with upper residual O_3 layers can explain this behavior. Sensitivity tests with a recurrent neural network model, using different subgroups of proxies, have been carried out and the results are shown in Fig. 6, where the observed and different simulated average diurnal O_3 mixing ratios are compared. The simulation that included all the proxies reproduced the observed O_3 mixing ratios for all hours of the day quite well, whereas a simulation that included only wind speed (a good proxy of atmospheric dynamics) reproduced the afternoon (after 15:00) and evening levels of O_3 with accuracy, missing the main O_3 peak before noon completely. In contrast, by using both wind speed and solar radiation as input parameters, the model reproduced the peak before noon and the high levels of afternoon–evening O_3 well. Putting together the results of these two simulations, we can conclude that the high level of O_3 during the afternoon is mainly due to dynamics (vertical intrusion from upper atmospheric layers and/or horizontal advection), for the following two reasons. (i) In the model, the wind speed used as input is enough to reproduce the afternoon concentrations of O_3 and (ii) the inclusion of solar radiation does not improve the agreement between measured and modeled O_3 during the afternoon, but substantially enhances the agreement between measurements and simulations before noon, when photochemistry, as expected, plays a larger role. The photochemistry contribution varied as a function of the hour of the day, ranging from 6 to 34 %.

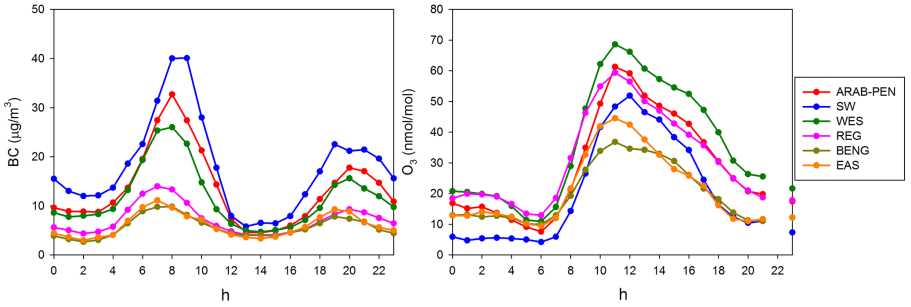

Figure 8. BC (left) and O_3 (right) diurnal variations as a function of the different air-mass clusters shown in Fig. 7. Abbreviations are as follows: ARAB-PEN – Arabian Peninsula, SW – southwesterly, WES – western, REG – regional, BENG – Bay of Bengal, and EAS – eastern.

3.5 Influence of atmospheric synoptic circulation

3.5.1 Synoptic-scale air-mass circulation scenarios

With the purpose of investigating the variability of large-scale atmospheric circulation affecting the region of interest, we clustered the HYSPLIT 5-day back trajectories. Here, it should be clearly stated that this analysis has been carried out with the aim of providing information about the synoptic-scale circulation scenarios which affect the region where the Kathmandu Valley is located, therefore investigating the link among these scenarios with the SLCF/P variability. In order to retain robust information, only the days for which the same cluster was observed for at least three-quarters of daily observations were considered in this analysis. Overall, nine clusters were identified; Fig. 7 shows the percentage of occurrence for each cluster for the whole investigation period, as a function of the different seasons. Three clusters out of nine had a very small percentage of occurrences (i.e., less than 5 % of air masses was recorded for each of these clusters), thus were not retained for further analysis (see Supplement). "Regional" (REG, 21.9 %) and "western" (WES, 21.4 %) clusters showed the highest occurrence values. The first encompasses trajectories within a $10° \times 10°$ area centered on the region of interest, thus indicating the occurrence of regional-scale atmospheric circulation: trajectories from this area were present in every season, except winter. WES, on the other hand, represents westerly air masses which originated (5 days backward in time) at a longitude around 60° E. The cyclonic behavior of these back trajectories indicated that synoptic-scale westerly disturbances could steer air masses under these scenarios. A significant fraction of trajectories (16.3 %), mostly observed during pre-monsoon and winter, showed westerly transport at the synoptic scale again (even if presenting higher horizontal velocities with respect to WES): 5-day back trajectories originated or traveled over desert areas of the Arabian Peninsula (ARAB-PEN). The larger latitudinal span of these back trajectories suggested that synoptic-scale disturbances and subtropical jet stream latitudinal excursions could steer the air masses towards the region of interest. During the monsoon and post-monsoon seasons, the atmospheric circulation was strongly affected by the summer monsoon and by the occurrence of low pressure areas in the Bay of Bengal, which enhanced the possibility to observe easterly circulation: i.e., "Bay of Bengal" (BENG, 12.8 %) and "Eastern" (EAS, 14.8 %) clusters. Finally, a non-negligible fraction of days (5.6 %, occurring mostly during winter) can be characterized by a southwesterly circulation (SW), which can be related to the passage of synoptic-scale disturbances over the western Indian subcontinent (Böhner, 2006). For more details and plots concerning the different back-trajectory clusters, please see the Supplement.

3.5.2 Influence of atmospheric circulation on O_3 and BC diurnal variations

The BC and O_3 diurnal variations, as a function of the different synoptic-scale air-mass circulation scenarios (Sect. 3.5.1) are shown in Fig. 8. The BC diurnal variation was only partly dependent on the air-mass clusters: the shape was the same for all of the clusters, although a difference in the amplitude of the cycles was recorded. In particular, regional air masses or on the eastern regions (BENG and EAS) were associated to smaller BC values both during peaks and minimum levels. This is because air masses from these regions were retrieved only during monsoon and post-monsoon seasons, when BC concentrations were at their minimum (no occurrences at all were registered during winter) due to enhanced wash-out. On the other hand, during winter and pre-monsoon, the highest values of BC were recorded under ARAB-PEN, WES, and SW air-mass circulation. Particularly, the diurnal cycle of BC and the relative 24h averaged peak values in the morning and in the evening were maximized when SW circulation affected the measurement site.

Concerning O_3 diurnal variation, significant differences can be observed as a function of different synoptic-scale circulation scenarios. Despite a moderate diurnal cycle of BC, the highest diurnal peak value and the largest amplitude of daily cycle were observed for the WES circulation; we

can hypothesize that air masses from the free troposphere or those that overpass polluted regions above the Indo-Gangetic Plain could contribute to the appearance of these high values. It is interesting to note that for the three synoptic-scale scenarios, most frequent during pre-monsoon and winter (i.e., WES, ARAB-PEN, and SW), very different results were obtained for BC and O_3. In particular, the diurnal peaks were maximized (minimized) for O_3 (BC). This can be tentatively explained by suggesting that under this circulation, meteorological conditions should favor the dilution of polluted air masses emitted from surface sources and transport of O_3-rich upper layers by vertical entrainment processes (e.g., Kleinman et al., 1994). Similar diurnal cycles but lower mixing ratios were tagged to ARAB-PEN and REG circulations. As for BC, the smallest O_3 diurnal cycles were linked to the typical monsoon circulations EAS and BENG: this is in agreement with Agrawal et al. (2008) who indicated that due to widespread rain precipitation and cloudy conditions, summer monsoon is not favorable to photochemical O_3 production and to the occurrence of elevated O_3 regime. With respect to other atmospheric circulation, the average O_3 diurnal cycles for ARAB-PEN, REG, and WES were characterized by high values from 13:00 to 21:00, while an intermediate condition was observed for the SW circulation.

3.5.3 Influence of open vegetation fires on BC and O_3 values

As shown in Putero et al. (2014), the BC and O_3 values in Nepal are partly influenced by the emissions from open vegetation fires, occurring across broad regions. In order to evaluate the contribution of large open fires emissions to the BC and O_3 variations observed at Paknajol, the daily total number of fires by the MODIS product has been retrieved and used. Fire pixels (with a confidence value $\geq 75\,\%$) were derived from the MODIS Global Monthly Fire Location Product (MCD14ML); these have been "filtered" by means of the MODIS Land Cover Climate Modeling Grid product (MCD12C1), in order to retain only fires occurring over specific land use categories (i.e., vegetation, croplands, forests; for more details on such products, see Justice et al., 2002; Friedl et al., 2010). This methodology did not allow us to account for the fraction that came from "residential" burning (e.g., garbage burning occurring in urban areas, or domestic burning). The study area for the open vegetation fires occurrences was the southern Himalayas box, 26–30° N, 80–88° E, considered in Putero et al. (2014) as the main contributor for Nepal. Over the whole period, the correlation coefficient between the number of fires and the delayed (from t to $t-3$ days) BC concentrations showed almost null correlation (0.10), pointing out that, in general, the BC fraction could be mainly influenced by other (local) anthropogenic emissions, also including the contribution from domestic and garbage burning. A sensitivity study was carried out by considering slightly different spatial domains for fire detection, without significant changes of the results. Nevertheless, some BC peaks have been superimposed to periods of high fire activities. During these events, the large-scale synoptic scenario, as deduced by HYSPLIT, showed WES and REG circulation, thus supporting the presence of regional-scale transport, and the possible influence from specific distinct (major) events of open vegetation fires. However, several limitations of the use of back trajectories and MODIS data (which can miss short-time events, small fires, and fires under clouds) have to be taken into account; for this reason, the use of chemical transport modeling outputs would be required for investigating these events in deeper detail. Figure 9 shows the diurnal BC and O_3 variations for the period of study (Fig. 9a–b) and the time series of total daily fires over the southern Himalayas box (as defined above) retrieved by MODIS (Fig. 9c).

BC diurnal variation seemed to remain quite constant over the entire time period, thus suggesting no prominent influence by fire emissions. During high fire activity periods (e.g., during the pre-monsoon season), BC showed increased concentrations, even though no shift of the daily maxima position occurred, thus indicating that local emissions (traffic and/or domestic, including open garbage burning) and PBL dynamic are the main factors influencing BC concentrations at Paknajol, further supported by the high ratio BC / PM_1. The same could not be said considering O_3 measurements. When the number of fires was at its highest, the O_3 peak was "shifted" in time and appeared in the late afternoon (between 16:00 and 18:00). This period almost perfectly matched with the "bump" in O_3 observed at the diurnal scale during the pre-monsoon season (Sect. 3.4). Here we hypothesize that biomass burning plumes that were enriched in O_3, photochemically produced after enhanced emission of precursors (e.g., CO, VOCs), could be transported over Kathmandu and possibly mixed within PBL due to efficient vertical mixing between upper ozone layers and surface layer.

4 Conclusions

In this work, we analyzed 1 full year of hourly-resolution data (February 2013–January 2014) of SLCF/P (BC and O_3) as well as aerosol number and mass concentration, observed at Paknajol, an urban site in the city center of Kathmandu, Nepal. Very high values of SLCF/P were detected during the whole measurement period, indicating persistent poor air quality conditions, dangerous for human health and the environment, including an influence on local/regional climate.

Equivalent BC, aerosol number concentration and aerosol mass concentration exhibited seasonal cycles, with the highest values during winter and pre-monsoon, and minima during the summer. Surface O_3 was characterized by maximum values during the pre-monsoon and a diurnal cycle (daytime maxima) opposite to what was observed for aerosol (midday minimum and maximum early in the morning and late evening). The diurnal behavior of BC and aerosol number

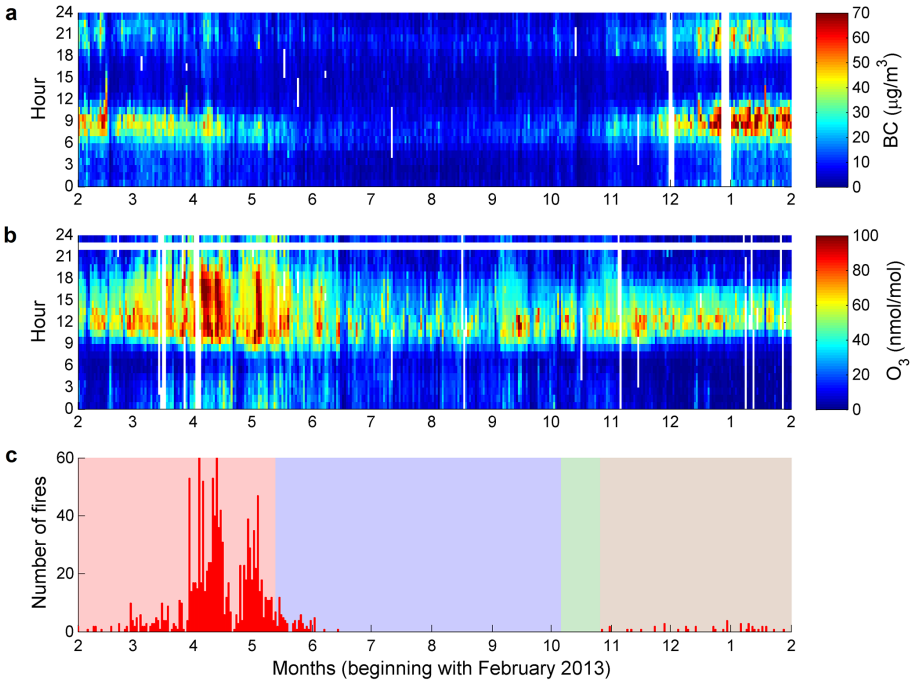

Figure 9. BC **(a)** and O_3 **(b)** diurnal variations over the entire sampling period. The color scale has been set to a maximum of 70 $\mu g\,m^{-3}$ and 100 $nmol\,mol^{-1}$ for BC and O_3, respectively. Panel **(c)** shows the total daily number of fires found in the southern Himalayas box (see Putero et al., 2014); note that the *y* axis has been limited to a maximum value of 60. Shaded areas in panel **(c)** indicate the different seasons (red: pre-monsoon, blue: monsoon, green: post-monsoon and brown: winter).

concentration indicated that local pollution sources, mostly related to road traffic or domestic emissions, represent the major contribution to air pollution in Kathmandu.

Concerning O_3, the analysis of the seasonal change of the diurnal cycle and correlation with meteorological parameters and aerosol properties suggested that apart from photochemistry (whose contribution ranges from 6 to 34 %), PBL dynamics and wind circulation have a significant role in determining O_3 variability: during midday, air masses richer in O_3 appeared to be transported to the measurement site by flows through the mountain passes located at the western rim of the Kathmandu Valley. Especially during pre-monsoon, high O_3 values were observed during the afternoon. We suggest that mixing and vertical entrainment processes between upper layers and PBL could partially explain the occurrence of these high values and can lead to favorable conditions for O_3 production that will often result in exceedance of guideline values set by the World Health Organization (WHO).

The possible impact of emissions by major open vegetation fires occurring at the regional scale has been assessed by analyzing MODIS fire distribution. A significant impact has been observed only for O_3 and during specific episodes, which is able to affect day-to-day variability. Despite the limitations of the methodology (e.g., garbage and domestic burning were not considered in this analysis and small or short-lasting open fires can be missed by satellite detection), this indicates that the occurrence of widespread biomass burning emissions can represent, in particular during the pre-monsoon season, a non-negligible source of precursors for O_3 photochemical production in the Kathmandu Valley.

The analysis of large-scale atmospheric circulation demonstrated a significant impact of the background synoptic-scale circulation on diurnal cycles of BC and O_3 in Kathmandu. In particular, atmospheric circulation related to westerly (WES, ARAB-PEN, SW) and regional (REG) circulations appeared to be especially conducive for the occurrence of the high BC and O_3 values.

Considering the 24 h limit of 120 $\mu g\,m^{-3}$ proposed for PM_{10} measurements by the Government of Nepal (Giri et al., 2006), we found for the 2013 period, a total of 124 exceedances, 51.4 % of the available PM_{10} data. In 2003, the Nepali Ministry of Population and Environment (MoPE) has also defined five different quality descriptions (classes) based on PM_{10} levels (see HMG/MOPE, 2003). During our observation period, following these references, 12 days (5 % of data) were categorized as "good" (range 0–60 $\mu g\,m^{-3}$), 105 as "moderate" (61–120 $\mu g\,m^{-3}$), and 103 days were tagged as "unhealthy" (121–350 $\mu g\,m^{-3}$), representing 43.6 and 42.7 % of data, respectively. A total of 21 days (8.7 %) were classified as "very unhealthy" (351–425 $\mu g\,m^{-3}$, 13 days) or "hazardous" ($> 425\,\mu g\,m^{-3}$, 8 days). Therefore, these data reveal the poor air quality in Kathmandu, also considering that the WHO guideline defines the limits of 20 $\mu g\,m^{-3}$ per year and 50 $\mu g\,m^{-3}$ per 24 h. WHO (2006) also defined air

quality guidelines for O_3 based on the analysis of the daily maximum 8h concentrations: high levels (HL: 240 µg m^{-3}), interim target-1 (IT-1: 160 µg m^{-3}), and air quality guidelines (AQG: 100 µg m^{-3}). Based on Paknajol data, we found 13 days that exceed the IT-1 (3.5 % of the data set) and 125 days (34 % of the data set) that exceed the AQG. It should be noted that WHO associated "important health effects" with IT-1 exceedances, indicating that exposures to the IT-1 level increase the number of attributable deaths by 3–5 %. Conversely, the exceedances of the AQG are related to an estimated 1–2 % increase in daily mortality (WHO, 2006). The totality of IT-1 exceedances were recorded during the pre-monsoon season; while AQG exceedances were observed for 62 % during the pre-monsoon, 22 % during the monsoon, and the remaining exceedances during post-monsoon (4 %) and winter (12 %). Roughly, the total number (97 %) of exceedances (IT-1 and AQG) were observed from 10:00 to 18:00. It is worth noting that 37 days (all detected during the pre-monsoon) were affected by the occurrence of major open vegetation fire activity during the investigated period. By neglecting these days, all of the IT-1 exceedances for O_3 at Paknajol were removed, and 88 AQG exceedances were retained (all the days with fire activity were tagged to AQG exceedances), representing a 29 % (47 %) decrease on a yearly (seasonal) basis.

The information of this study, developed in the framework of the SusKat-ABC project, may be useful for implementing control measures to mitigate the occurrence of acute pollution levels in the Kathmandu municipality, as well as for improving regional climate conditions. This is important for the wider area that lies at the Himalayan foothills.

The Supplement related to this article is available online at doi:10.5194/acp-15-13957-2015-supplement.

Acknowledgements. This work was supported by the National Project NextData, funded by the Italian Ministry of Education, University and Research. The authors thank the Institute for Advanced Sustainability Studies (IASS) and the International Centre for Integrated Mountain Development (ICIMOD) that led the Sustainable Atmosphere for the Kathmandu Valley (SusKat) project. This study was partially supported by core funds of ICIMOD, contributed by the governments of Afghanistan, Australia, Austria, Bangladesh, Bhutan, China, India, Myanmar, Nepal, Norway, Pakistan, Switzerland, and the United Kingdom.

Edited by: R. Müller

References

Agrawal, M., Auffhammer, M., Chopra, U. K., Emberson, L., Iyngararasan, M., Kalra, N., Ramana, M. V., Ramanathan, V., Singh, A. K., and Vincent, J.: Impacts of Atmospheric Brown Clouds on agriculture, Part II of Atmospheric Brown Clouds: regional assessment report with focus on Asia, Project Atmospheric Brown Cloud, UNEP, Nairobi, Kenya, 2008.

Alastuey, A., Querol, X., Castillo, S., Escudero, M., Avila, A., Cuevas, E., Torres, C., Romero, P.-M., Exposito, F., Garcia, O., Diaz, J. P., Van Dingenen, R., and Putaud, J. P.: Characterisation of TSP and PM2.5 at Izaña and Sta. Cruz de Tenerife (Canary Islands, Spain) during a Saharan Dust Episode (July 2002), Atmos. Environ., 39, 4715–4728, 2005.

Aryal, R. K., Lee, B.-K., Karki, R., Gurung, A., Kandasamy, J., Pathak, B. K., Sharma, S., and Giri, N.: Seasonal PM_{10} dynamics in Kathmandu valley, Atmos. Environ., 42, 8623–8633, 2008.

Biancofiore, F., Verdecchia, M., Di Carlo, P., Tomassetti, B., Aruffo, E., Busilacchio, M., Bianco, S., Di Tommaso, S., and Colangeli, C.: Analysis of surface ozone using a recurrent neural network, Sci. Total Environ., 514, 379–387, 2015.

Böhner, J.: General climatic controls and topoclimatic variations in Central and High Asia, Boreas, 35, 279–294, 2006.

Bonasoni, P., Laj, P., Marinoni, A., Sprenger, M., Angelini, F., Arduini, J., Bonafè, U., Calzolari, F., Colombo, T., Decesari, S., Di Biagio, C., di Sarra, A. G., Evangelisti, F., Duchi, R., Facchini, M. C., Fuzzi, S., Gobbi, G. P., Maione, M., Panday, A., Roccato, F., Sellegri, K., Venzac, H., Verza, G. P., Villani, P., Vuillermoz, E., and Cristofanelli, P.: Atmospheric Brown Clouds in the Himalayas: first two years of continuous observations at the Nepal Climate Observatory-Pyramid (5079 m), Atmos. Chem. Phys., 10, 7515–7531, doi:10.5194/acp-10-7515-2010, 2010.

Chevalier, A., Gheusi, F., Delmas, R., Ordóñez, C., Sarrat, C., Zbinden, R., Thouret, V., Athier, G., and Cousin, J.-M.: Influence of altitude on ozone levels and variability in the lower troposphere: a ground-based study for western Europe over the period 2001–2004, Atmos. Chem. Phys., 7, 4311–4326, doi:10.5194/acp-7-4311-2007, 2007.

Claiborn, C. S., Finn, D., Larson, T. V., and Koenig, J. Q.: Windblown dust contributes to high PM2.5 concentrations, J. Air Waste Ma., 50, 1440–1445, 2000.

Colbeck, I., Nasir, Z. A., Ahmad, S., and Ali, Z.: Exposure to PM10, PM2.5, PM1 and Carbon Monoxide on roads in Lahore, Pakistan, Aerosol Air Qual. Res., 11, 689–695, 2011.

Cozic, J., Verheggen, B., Mertes, S., Connolly, P., Bower, K., Petzold, A., Baltensperger, U., and Weingartner, E.: Scavenging of black carbon in mixed phase clouds at the high alpine site Jungfraujoch, Atmos. Chem. Phys., 7, 1797–1807, doi:10.5194/acp-7-1797-2007, 200.

Cristofanelli, P., Bracci, A., Sprenger, M., Marinoni, A., Bonafè, U., Calzolari, F., Duchi, R., Laj, P., Pichon, J. M., Roccato, F., Venzac, H., Vuillermoz, E., and Bonasoni, P.: Tropospheric ozone variations at the Nepal Climate Observatory-Pyramid (Himalayas, 5079 m a.s.l.) and influence of deep stratospheric intrusion events, Atmos. Chem. Phys., 10, 6537–6549, doi:10.5194/acp-10-6537-2010, 2010.

Deshmukh, D. K., Deb, M. K., and Verma, S. K.: Distribution patterns of coarse, fine and ultrafine atmospheric aerosol particulate matters in major cities of Chhattisgarh, Indian J. Environ. Prot., 30, 184–197, 2010.

Deshmukh, D. K., Deb, M. K., and Mkoma, S. L.: Size distribution and seasonal variation of size-segregated particulate matter

in the ambient air of Raipurcity, India, Air Qual. Atmos. Health, 6, 259–276, 2013.

Di Carlo, P., Pitari, G., Mancini, E., Gentile, S., Pichelli, E., and Visconti, G.: Evolution of surface ozone in central Italy based on observations and statistical model, J. Geophys. Res., 112, D10316, doi:10.1029/2006JD007900, 2007.

Draxler, R. R.: HYSPLIT4 user's guide. NOAA Tech. Memo. ERL ARL-230, NOAA Air Resources Laboratory, Silver Spring, MD, 1999.

Draxler, R. R. and Hess, G. D.: An overview of the HYSPLIT_4 modelling system for trajectories, dispersion and deposition, Aust. Meteorol. Mag., 47, 295–308, 1998.

Elman, L. J.: Finding structure in time, Cognitive Sci., 14, 179–211, 1990.

Faiz, A., Ale, B. B., and Nagarkoti, R. K.: The role of inspection and mainteinance in controlling vehicular emissions in Kathmandu Valley, Nepal, Atmos. Environ., 40, 5967–5975, 2006.

Friedl, M. A., Sulla-Menashe, D., Tan, B., Schneider, A., Ramankutty, N., Sibley, A., and Huang, X.: MODIS Collection 5 global land cover: algorithm refinements and characterization of new datasets, Remote Sens. Environ., 114, 168–182, 2010.

Gilge, S., Plass-Duelmer, C., Fricke, W., Kaiser, A., Ries, L., Buchmann, B., and Steinbacher, M.: Ozone, carbon monoxide and nitrogen oxides time series at four alpine GAW mountain stations in central Europe, Atmos. Chem. Phys., 10, 12295–12316, doi:10.5194/acp-10-12295-2010, 2010.

Giri, D., Murthy, K., Adhikary, P. R., and Khanal, S. N.: Ambient air quality of Kathmandu valley as reflected by atmospheric particulate matter concentrations (PM_{10}), Int. J. Environ. Sci. Te., 3, 403–410, 2006.

HMG/MOPE: Draft report on air emission inventory, Kathmandu, Nepal, 2003.

Hyvärinen, A.-P., Vakkari, V., Laakso, L., Hooda, R. K., Sharma, V. P., Panwar, T. S., Beukes, J. P., van Zyl, P. G., Josipovic, M., Garland, R. M., Andreae, M. O., Pöschl, U., and Petzold, A.: Correction for a measurement artifact of the Multi-Angle Absorption Photometer (MAAP) at high black carbon mass concentration levels, Atmos. Meas. Tech., 6, 81–90, doi:10.5194/amt-6-81-2013, 2013.

India Meteorological Department (IMD): Monsoon report 2013, edited by: Pai, D. S. and Bhan, S. C., Pune, India, 2014.

Jacobson, M. Z.: Atmospheric pollution: history, science and regulation, Cambridge University Press, Cambridge, United Kingdom and New York, NY, USA, 2002.

Justice, C. O., Giglio, L., Korontzi, S., Owens, J., Morisette, J. T., Roy, D., Descloitres, J., Alleaume, S., Petitcolin, F., and Kaufman, Y.: The MODIS fire products, Rem. Sens. Environ., 83, 244–262, 2002.

Klausen, J., Zellweger, C., Buchmann, B., and Hofer, P.: Uncertainty and bias of surface ozone measurements at selected Global Atmosphere Watch sites, J. Geophys. Res., 108, 4622, doi:10.1029/2003JD003710, 2003.

Kleinman, L., Lee, Y.-N., Springston, S. R., Nunnermacker, L., Zhou, X., Brown, R., Hallock, K., Klotz, P., Leahy, D., Lee, J. H., and Newman, L.: Ozone formation at a rural site in the southeastern United States, J. Geophys. Res., 99, 3469–3482, 1994.

Lönnblad, L., Peterson, C., and Röngvalsson, T.: Pattern recognition in high energy physics with artificial neural network – Jetnet 2.0, Comput. Phys. Commun., 70, 167–182, 1992.

Lundgren, D. A., Hlaing, D. N., Rich, T. A., and Marple, V. A.: PM10/PM2.5/PM1 data from a trichotomous sampler, Aerosol Sci. Tech., 25, 353–357, 1996.

Marinoni, A., Cristofanelli, P., Laj, P., Duchi, R., Calzolari, F., Decesari, S., Sellegri, K., Vuillermoz, E., Verza, G. P., Villani, P., and Bonasoni, P.: Aerosol mass and black carbon concentrations, a two year record at NCO-P (5079 m, Southern Himalayas), Atmos. Chem. Phys., 10, 8551–8562, doi:10.5194/acp-10-8551-2010, 2010.

Monks, P. S., Granier, C., Fuzzi, S., Stohl, A., Williams, M. L., Akimoto, H., Amann, M., Baklanov, A., Baltensperger, U., Bey, I., Blake, N., Blake R. S., Carslaw, K., Cooper O. R., Dentener, F., Fowler, D., Fragkou, E., Frost, G. J., Generoso, S., Ginoux, P., Grewe, V., Guenther, A., Hansson, H. C., Henne, S., Hjorth, J., Hofzumahaus, A., Huntrieser, H., Isaksen, I. S. A., Jenkin, M. E., Kaiser, J., Kanakidou, M., Klimont, Z., Kulmala, M., Lawrence, M. G., Lee, J. D., Liousse, C., Maione, M., and McFiggans, G.: Atmospheric composition change – global and regional air quality, Atmos. Environ., 43, 5268–5350, 2009.

Panday, A. and Prinn, R. G.: Diurnal cycle of air pollution in the Kathmandu Valley, Nepal: Observations, J. Geophys. Res., 114, D09305, doi:10.1029/2008JD009777, 2009.

Panday, A., Prinn, R. G., and Schär, C.: Diurnal cycle of air pollution in the Kathmandu Valley, Nepal: 2. Modeling results, J. Geophys. Res., 114, D21308, doi:10.1029/2008JD009808, 2009.

Pudasainee D., Balkrishna S., Shrestha, M. L., Kaga, A., Kondo, A., and Inoue, Y.: Ground level ozone concentrations and its association with NOx and meteorological parameters in Kathmandu valley, Nepal, Atmos. Environ., 40, 8081–8087, 2006.

Putero, D., Landi, T. C., Cristofanelli, P., Marinoni, A., Laj, P., Duchi, R., Calzolari, F., Verza, G. P., and Bonasoni, P.: Influence of open vegetation fires on black carbon and ozone variability in the southern Himalayas (NCO-P, 5079 m a.s.l.), Environ. Pollut., 184, 597–604, 2014.

Ramanathan, V. and Carmichael, G.: Global and regional climate changes due to black carbon, Nat. Geosci., 1, 221–227, 2008.

Ramanathan, V., Li, F., Ramana, M. V., Praveen, P. S., Kim, D., Corrigan, C. E., Nguyen, H., Stone, E. A., Schauer, J. J., Carmichael, G. R., Adhikary, B., and Yoon, S. C.: Atmospheric brown clouds: Hemispherical and regional variations in long-range transport, absorption, and radiative forcing, J. Geophys. Res., 112, D22S21, doi:10.1029/2006JD008124, 2007.

Rupakheti, M., Panday, A. K., Lawrence, M. G., Kim, S. W., Sinha, V., Kang, S. C., Naja, M., Park, J. S., Hoor, P., Holben, B., Bonasoni, P., Sharma, R. K., Mues, A., Mahata, K., Bhardwaj, P., Sarkar, C., Rupakheti, D., Regmi, R. P., and Gustafsson, Ö.: Air pollution in the Himalayan foothills: Overview of the SusKat-ABC international air pollution measurement campaign in Nepal, Atmos. Chem. Phys. Discuss., in preparation, 2015.

Shahsavani, A., Naddafi, K., Jafarzade Haghighifard N., Mesdaghinia, A., Yunesian, M., Nabizadeh, R., Arahami, M., Sowlat, M. H., Yarahmadi, M., Saki, H., Alimohamadi, M., Nazmara, S., Motevalian, S. A., and Goudarzi, G.: The evaluation of PM10, PM2.5 and PM1 concentrations during the Middle Eastern Dust (MED) events in Ahvaz, Iran, from april through September 2010, J. Arid Environ., 77, 72–83, 2012.

Sharma, C. K.: Urban air quality of Kathmandu Valley "Kingdom of Nepal", Atmos. Environ., 31, 2877–2883, 1997.

Sharma, R. K., Bhattarai, B. K., Sapkota, B. K., Gewali, M. B., and Kjeldstad, B: Black carbon aerosols variation in Kathmandu valley, Nepal, Atmos. Environ., 63, 282–288, 2012.

Shindell, D., Kuylenstierna, J. C. I., Vignati, E., van Dingenen, R., Amann, M., Klimont, Z., Anenberg, S. C., Muller, N., Janssens-Maenhout, G., Raes, F., Schwartz, J., Faluvegi, G., Pozzoli, L., Kupiainen, K., Höglund-Isaksson, L., Emberson, L., Streets, D., Ramanathan, V., Hicks, K., Kim Oanh, N. T., Milly, G., Williams, M., Demkine, V., and Fowler, D.: Simultaneously mitigating near-term climate change and improving human health and food security, Science, 335, 183–189, 2012.

Shrestha, P., Barros, A. P., and Khlystov, A.: Chemical composition and aerosol size distribution of the middle mountain range in the Nepal Himalayas during the 2009 pre-monsoon season, Atmos. Chem. Phys., 10, 11605–11621, doi:10.5194/acp-10-11605-2010, 2010.

Shrestha, R. M. and Malla, S.: Air pollution from energy use in a developing country city: the case of Kathmandu Valley, Nepal, Energy, 21, 785–794, 1996.

Shrestha, R. M. and Rajbhandari, S.: Energy and environmental implications of carbon emission reduction targets: Case of Kathmandu Valley, Nepal, Energ. Policy, 38, 4818–4827, 2010.

Shrestha, S. R., Kim Oanh, N. T., Xu, Q., Rupakheti, M., and Lawrence, M. G.: Analysis of the vehicle fleet in the Kathmandu Valley for estimation of environment and climate co-benefits of technology intrusions, Atmos. Environ., 81, 579–590, 2013.

UNEP and WMO: Integrated Assessment of Black Carbon and Tropospheric Ozone, UNEP, Nairobi, 2011.

Wang, G., Wang, H., Yu, Y., Gao, S., Feng, J., Gao, S., and Wang, L.: Chemical characterization of water-soluble components of PM10 and PM2.5 atmospheric aerosols in five locations of Nanjing, China, Atmos. Environ., 37, 2893–2902, 2003.

World Health Organization: WHO Air quality guidelines for particulate matter, ozone, nitrogen dioxide and sulfur dioxide, Global update 2005, Summary of risk assessment, WHO Press, Geneva, Switzerland, 2006.